A Family of Isostructural Mononuclear Trigonal Bipyramidal Cobalt Single Molecule Magnets.

Toby J. Woods,† María F. Ballesteros-Rivas,†‡ Silvia Gómez-Coca,† Eliseo Ruiz§ and Kim R. Dunbar†

†Department of Chemistry, Texas A&M University, College Station, TX, 77842, United States.

§Departament de Química Inorgànica i Orgànica and Institut de Recerca en Química Teòrica i Computacional, Universitat de Barcelona, Barcelona, 08028, Spain.

KEYWORDS (Word Style "BG_Keywords"). If you are submitting your paper to a journal that requires keywords, provide significant keywords to aid the reader in literature retrieval.

ABSTRACT: A family of isostructural, mononuclear Co^{II} complexes have been synthesized in which the Co^{II} ions reside in distorted trigonal bipyramidal coordination environments. The degree of distortion as well as the overall symmetry of the molecule was varied across members of the series. By magnetostructural correlations and ab initio calculations it has been determined that the deciding factor for SMM behavior is not the degree of distortion but the interactions between neighboring molecules in the solid state.

INTRODUCTION

The search for compounds systems that exhibit SMM behavior continues but focus has shifted from the large spin ground state molecules synthesized in the early days of the field to smaller molecules, including mononuclear systems. This trend reflects the fact that controlling magnetic anisotropy, which is crucial for determining the energy barrier to spin reversal, is simplified when there is only one spin-bearing metal ion. In fact there are numerous reports in the literature regarding the SMM behavior of complexes containing a single lanthanide ion[1-3] and reports of SMM behavior for mononuclear complexes are increasing rapidly.[4-11] The library of mononuclear Co^{II} SMMs has recently been expanded to include a seven-coordinate pentagonal bipyramidal complex[12] and an eight-coordinate square antiprismatic complex.[13] The highest reported effective energy barrier to date for a mononuclear Co^{II} complex is 322 cm^{-1} for the four-coordinate $(HNEt_3)_2[Co^{II}(L^{2-})_2]$ (H_2L = 1,2-bis(methanesulfonamido)benzene).[14] Several mononuclear iron complexes[15-17] and, very recently, mononuclear Ni^{I} complexes[18,19] as well as a mononuclear Ni^{III} SMM[20] have been reported. Herein we describe our efforts to exploit the single-ion anisotropy of Co^{II} in mononuclear complexes that have the potential for being used as secondary building units for heterometallic coordination complexes. In this approach, the Co^{II} ion is capped by an organic ligand to limit the dimensionality of the resulting complex, specifically the TPMA ligand. The series of mononuclear complexes of general formula $[Co(TPMA)X]_{n+}(Y)_m$ (TPMA = tris(2-pyridylmethyl)amine, X = CH_3CN, n = 2, Y = BF_4, m = 2; X = Cl, Br, I, n = 1, Y = Cl, Br, I, m = 1) were synthesized in which the Co^{II} ion resides in a trigonal bipyramidal (TBP) environment with the axial ligand being CH_3CN, $[Cl]^-$, $[Br]^-$, or $[I]^-$, which should be easily replaced upon reaction with a suitable metal precursor. TPMA was chosen as the capping ligand to provide a rigid backbone for the cobalt center while still leaving an open coordination site for further chemistry to occur.

RESULTS AND DISCUSSION

Synthesis and structures

A series of six complexes, $[Co(TPMA)(CH_3CN)](BF_4)_2{\cdot}CH_3CN$ (**1**), $[Co(TPMA)Cl]Cl{\cdot}2.4H_2O$ (**2t**), $[Co(TPMA)Cl]Cl$ (**2c**), $[Co(TPMA)Br]Br{\cdot}2H_2O$ (**3t**), $[Co(TPMA)Br]Br$ (**3c**), and $[Co(TPMA)I]I$ (**4**), have been synthesized by simple reaction between TPMA and a suitable Co^{II} precursor. **1** crystallizes in the monoclinic space group *P2₁/c*, **2c** and **3c** crystallize in the cubic space group *P2₁3*, and **2t**, **3t**, and **4** crystallize in the triclinic space group *P-1*. For **2t** and **3t** the stated water content is an average of the water content as determined by thermogravimetric and elemental analyses. The asymmetric unit of **1**, **2c** and **3c** contain one crystallographically independent molecule while **4** contains two and **2t** and **3t** contain three crystallographically independent molecules. Details of the X-ray structural refinements are contained in the Supplementary Information.

The coordination sphere of the Co^{II} ions in all of the complexes consists of the four nitrogen atoms from the TPMA capping ligand and either one nitrogen atom from a coordinated CH_3CN molecule or a coordinated halide ion, resulting in a TBP coordination environment. Using the Shape program,añadir referencias which compares the

coordination geometry of the studied molecule to a perfect coordination environment, all the members of this family are best described as trigonal bipyramidal molecules with the equatorial plane defined by the three pyridine N atoms of TPMA and where the Co ion is situated slightly below this N3 plane (Figure 1). The Shape value (S) with respect to the TBP geometry (Table S3) was found to vary between 0.97 for **1** and 3.24 for **4** (S is equal to 0 for a perfect TBP geometry). The increase in the S value when descending in the halide series is principally due to the increase in the Co-X distance.

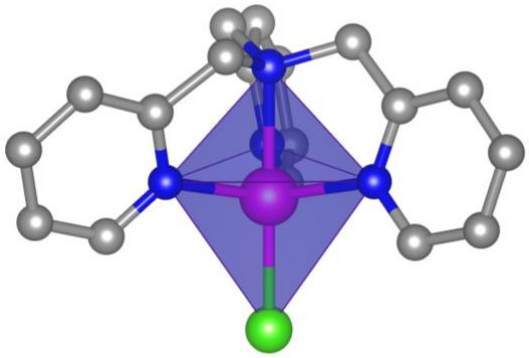

Figure 1. Molecular structure of compound **2c** showing the trigonal bipyramidal geometry (purple polyhedra) with the equatorial plane defined by the three pyridine N atoms of TPMA. Cobalt, chlorine, nitrogen and carbon are in pink, green, blue, and grey, respectively. Hydrogen atoms have been omitted for clarity.

All members of the family exhibit approximate C_3 symmetry, with the cubic phases (**2c** and **3c**) having crystallographically imposed C_3 symmetry. As can be seen in Figure 2, if only the first coordination sphere is considered, the molecules have C_{3v} symmetry. The mirror plane symmetry is broken by the slight tilt of the pyridine rings and non-planarity between the methyl carbon atom connecting the pyridine rings to the bridgehead amine nitrogen atom and the pyridine rings themselves. For complexes **1** – **4** the Co^{II} ion projects out of the N3 plane formed by the TPMA pyridine rings toward the terminal halide or CH_3CN ligand, resulting in N_{py}-Co-N_{amine} angles of less than 90°. This distortion also leads to deviations in the equatorial bond angles away from 120°. A list of pertinent bond distances and angles is given in Table S2.

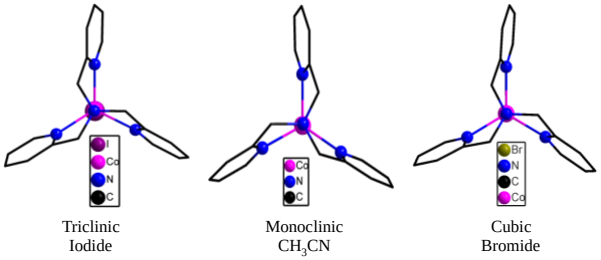

Figure 2. View down the C_3 axis of representative members of the $[Co(TPMA)X]^{1+/2+}$ series.

No me gusta mucho lo de las bolas de colores en el dibujo, àra mi mejor en el caption, especialmente que solo hay bolas para el N y el Co, no para los C…

For the triclinic phases of [Co(TPMA)Cl]Cl and [Co(TPMA)Br]Br, **2t** and **3t** respectively, outer-sphere halide and water oxygen atoms were found to be disordered over multiple positions. Details of the methods used to refine the site occupancy of the halide and water oxygen atoms can be found in the Supplemental Information. Powder X-ray diffraction (Supporting Information Figures S1-S3) was used to verify the phase purity of each bulk sample prior to conducting magnetic measurements.

DC magnetic measurements

Static DC magnetic measurements were performed on crushed single crystals of **1** – **4** between 1.8 and 300 K (Figure 3). The behavior is similar for all six compounds. At 300 K the χT value is ~2.4 emu K mol^{-1}, significantly higher than the 1.875 emu K mol^{-1} expected for an S = 3/2 system with g = 2, an indication of single-ion anisotropy within the Co^{II} ion.

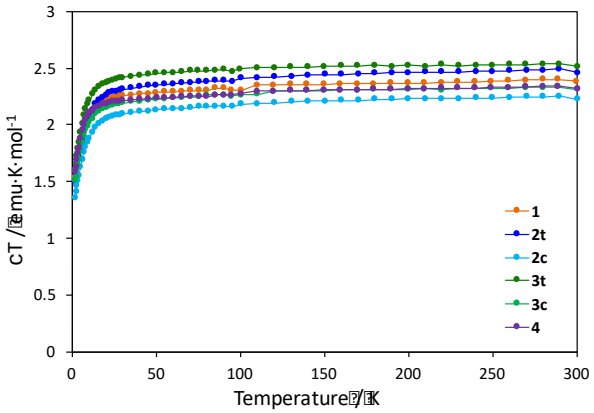

Figure 3. Magnetic susceptibility vs temperature under a 1000 Oe applied field for compounds **1** – **4**.

Additionally, M vs. H measurements at 1.8 K did not saturate at the highest available field of 7 T, a further indication of a high degree of anisotropy in these systems. Reduced magnetization data for **1** – **4** were recorded between 1.8 and 4 K (Figures S6 – S11). The results of fitting the field-dependent magnetization data using PHI[21] are shown in Table 1, along with the results of *ab initio* calculations (*vida infra*). For **1**, attempts to fit the field-dependent magnetization data with negative values of D resulted in lower-quality fits of the data, only a positive D value provides a reasonable fitting; the small value of the transverse anisotropy parameter E is appropriate for a molecule of C_3 symmetry.[4] For **2** through **4**, the fits to the magnetization data are better with negative D values. For **2c**, the sign and magnitude of D as well as the g value are consistent with the ZFS parameters derived from EPR studies of $[Co(Me_6tren)Cl](ClO_4)$, which crystallizes in the trigonal space group *R3c*.[4] The similarity in the ZFS parameters between the triclinic and cubic phases **2t** and **2c** suggests that the electronic environment is not significantly affected by the pseudo-C_3 symmetry of the triclinic phase versus the rigorous C_3 symmetry of the cubic phase. For **3c**, the sign of D is consistent with that reported for $[Co(Me_6tren)Br]Br$ as derived from EPR studies[4] but is larger in magnitude, namely -2.4 cm^{-1} for

[Co(Me$_6$tren)Br]Br as compared to -7.2 cm^{-1} for **3c**. The smaller D value for [Co(Me$_6$tren)Br]Br as compared to [Co(Me$_6$tren)Cl]$^+$ was attributed to a stronger σ-donor effect from the equatorial amine nitrogen atoms of Me$_6$tren as evidenced by shortened Co-N$_{amine}$ bond lengths. The authors provided computational evidence that this increase in σ donation has the effect of increasing the energy gap between the (d_{xz},d_{yz}) and (d_{xy},d_{x2-y2}) orbital sets, leading to a smaller D value. Un diagrama de orbitals por aquí iría bien…The TPMA ligand is more rigid than Me$_6$tren as evidenced by only minor changes in the Co-TPMA bonding metrics among all members of the family thus making the energy gap between the (d_{xz},d_{yz}) and (d_{xy},d_{x2-y2}) orbital sets relatively constant across the series, leading to similar values for D across the series. Similar to the chloride analogs, the ZFS parameters for the triclinic bromide phase **3t** are quite close to those obtained for the cubic phase **3c**. For **4**, fits of similar quality to the reported negative D value could be obtained with a positive D value of similar magnitude and a slightly lower g value. We have chosen to report the negative D value based on the results of the *ab initio* calculations.

Table 1. Experimental and calculated (CASSCF+spin orbit) ZFS parameters (in cm^{-1}) and g values for compounds 1 - 4.

	Experimental			Calculated		
Compound	D	E	g_{iso}	D	|E|	g_{iso}
1	9.66	0.26	2.39	8.86	0.98	2.23
2t	-6.95	-1.78	2.25	-7.47	0.42	2.26
2c	-8.49	0.0	2.30	-8.63	0.0	2.27
3t	-6.30	1.59	2.34	-4.83	0.41	2.27
3c	-7.18	0.0	2.23	-5.30	0.0	2.27
4	-7.53	1.00	2.37	-2.97	0.66	2.27

AC magnetic measurements

Dynamic AC magnetic measurements on **1** – **4** have been performed as a function of the applied DC field (Figure 4). Only compound **2c** shows an out-of-phase signal without an applied DC field in the form of a tail at higher frequencies; no maximum in χ'' was observed. Compounds **2t**, **3t** and **4** revealed a non-zero signal in χ'' at high frequencies but no maximum in the out-of-phase component was observed. **1**, **2c** and **3c**, however, revealed clear SMM behavior in the presence of an applied DC field. Compound **2c** is the one showing a maximum at lower frequencies (around 20 Hz), followed by compound **1** with a maximum around 90 Hz. However, for **3c** the maximum is only observed at higher frequencies, larger than 100 Hz. For **1**, **2c** and **3c** the fitting of the Cole-Cole plot using a modified Debye function[22,23] was performed, allowing for the extraction of the τ and α parameters, Figures S12-S15 and Tables S4-S7. For **2c** there is also a distinct tail at high frequencies indicative of a second relaxation process. To evaluate this tail the fitting of the Cole-Cole plot has been done using only the frequencies from 10 to 415 Hz and by using two relaxation processes. Both procedures give almost identical parameters for the predominant process at lower frequencies. The fitting of τ vs field at 1.8 K with an equation including direct and tunneling relaxation processes and a constant to include the processes with no field dependence is shown in the SI (Equation S1, Figures S16-S18 and Table S8). No entiendo en la ecuación S1 del SI porque en el termino directo no hay el valor de T (1.8 multiplicando) For the optimum field the value of τ^{-1} is predominantly described by the constant parameter. At smaller fields, the decrease of τ^{-1} with field can be ascribed to tunneling. For **2c** the increase of τ^{-1} with field at higher fields can be attributed to a direct process.

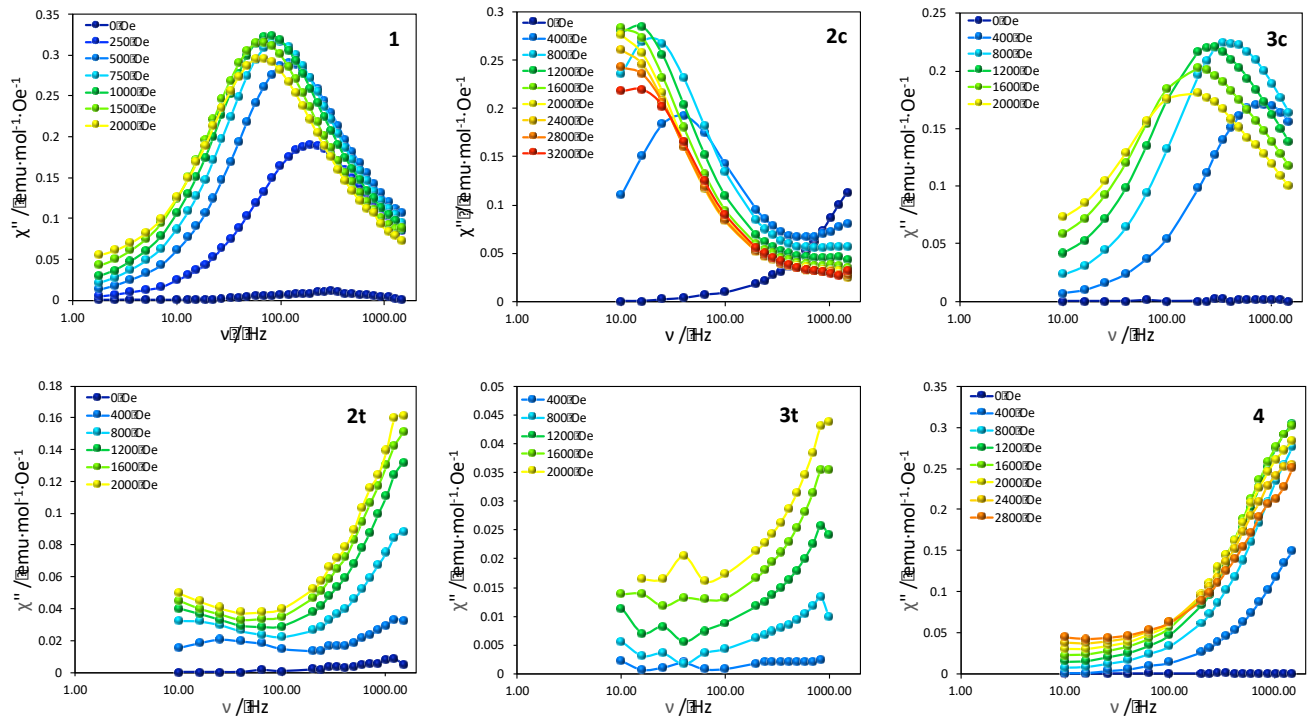

Figure 4. AC magnetic measurements for **1** – **4** at 1.8 K and different applied DC magnetic fields.

In an applied DC field of 1000 Oe, frequency-dependent maxima in χ'' were observed below 2.4 K for **1** (Figure 5). A fitting of the Cole-Cole plot using a modified Debye function[22,23] allowed for the extraction of the τ and α parameters, Figure S19 and Table S9. The τ values were used to construct an Arrhenius plot (Figure 6), from which the relaxation parameters of U_{eff}/k_b = 21 K and τ_o = 1.7 x 10^{-8} s were determined. The barrier to thermal relaxation in **1** is slightly higher than the 18 K barrier reported for $[Co(Me_6tren)(OH_2)]^{2+}$ with τ_o = 9.6 x 10^{-9} s.[5] The α parameter in **1** varies between 0.14 and 0.16, indicating a relatively narrow distribution of relaxation times. What is intriguing about this complex is that there is no evidence of a crossover to a quantum tunneling regime at low temperatures. Among the previously reported mononuclear Co^{II} SMMs the observation of a tunneling regime at low temperatures is more common than observing thermal spin relaxation down to the lowest measured temperature.[5-9,24-34] Application of a 1000 Oe DC bias field appears to be sufficient for blocking the tunneling pathway at all temperatures above 1.8 K. Since the splitting between the M_s = ±1/2 and ±3/2 sublevels is 2|***D***| in this case, a purely thermal relaxation pathway should lead to an energy barrier of 28 K, only slightly higher than the observed U_{eff}/k_b of 21.0 K. This fact further supports that tunneling is not a major relaxation pathway above 1.8 K. To further verify the Orbach mechanism's predominance over other processes a fit including tunneling, direct, and Raman processes has been performed (Equation S2). To avoid overparametrization of the fitting the tunneling and direct parameters have been fixed to those previously obtained in the fitting of the dependence of τ^{-1} with field. The fit shows a clear predominance of the Orbach process with a small contribution from tunneling (Figure S29 and Table S15) giving U_{eff}/k_b = 23.8 K, slightly closer to the expected value of 28 K.

Previous reports of Co^{II} SMMs with a large rhombic term have put forth the hypothesis that slow relaxation is due to the rhombic term establishing an "easy axis" within the easy plane.[35,36] As the rhombic term is very small in **1** **explain why?** this does not seem to be a viable explanation for the SMM behavior in this case. A pseudo-tetrahedral mononuclear Co^{II} complex with a positive D value and a low E value reported by Long and co-workers displays SMM behavior in which thermal relaxation was observed instead of direct tunneling between the M_s = ±1/2 states which was attributed to a phonon bottleneck effect, namely there are not enough phonon modes of the proper frequency to allow for tunneling.[28] A more recent report from the Ruiz and Luis groups has demonstrated that the inclusion of the hyperfine coupling (I = 7/2 for Co) and the nuclear spin-lattice interaction is necessary to explain the spin relaxation in Co^{II} systems with easy-plane anisotropy.[37]

For compound **2c**, in a 400 Oe DC field there are frequency dependent maxima in χ'' for frequencies as low as 33 Hz at 1.8 K but there is also a distinct tail at high frequencies indicative of a second relaxation process (Figure S20). This tail becomes less apparent at higher temperatures and by 2.3 K it has disappeared. Attempts to use a single modified Debye function could not reproduce these tails and, in general, resulted in unsatisfactory fits to the data. Using CC-FIT,[38] both relaxation processes were fit simultaneously (Figure S21 and Table S10). One of the relaxation processes, τ_1 in Figure S27, appears to be essentially temperature independent, consistent with quantum tunneling, but no further interpretation of this process is possible since no maximum in χ'' was observed.

The second process, τ_2, produces the linear Arrhenius plot shown in Figure S27. This relaxation process is frequency dependent at all measured temperatures, consistent with a thermal relaxation process. The effective barrier extracted for this thermal process is 20.6 K with a pre-exponential factor of 4.43 x 10^{-8} s. The alpha values are all less than 0.07, indicating a narrow distribution of relaxation times. The observed barrier is consistent with the one calculated from $(S^2 - {}^1/_4)|D|$ (24 K); the barrier height is also consistent with the energy gap of $2|D|$ (24 K) between the $M_S = \pm {}^3/_2$ and $M_S = \pm {}^1/_2$ states, in accord with the relaxation pathway being via an Orbach process.

To further validate the fitted parameters for the thermal process, another fitting of the 400 Oe Cole-Cole data was performed with CC-FIT that did not include the five highest AC frequencies, which minimized the appearance of a tail in the Cole-Cole plot at 1.8 K and virtually eliminated the tail at all higher temperatures. The results of this fitting are shown in Figure S22 and Table S11. The value of U_{eff}/k_b extracted from this fitting was 21.3 K with τ_o = 2.98 x 10^{-8} s. The alpha values range from 0.12 at 1.8 K to 0.02 at 2.7 K. These results are consistent with the values obtained from the fitting using two relaxation processes and demonstrate that the tail observed in the Cole-Cole plot is due to a second, fast relaxation process that has little effect on the thermal relaxation mechanism that is observed at high temperatures.

Table 2. Experimental relaxation parameters for compounds 1, 2c and 3c at different applied fields together with the experimental D values (in K). Maybe add here the values from the new fit using other processes…

Compound	Field (Oe)	U_{eff}/k_b (K)	τ_o (s)	D (K)
1	1000	21.0	1.7 x 10^{-8}	13.9
2c	400	21.3	2.98 x 10^{-8}	12.2
	2000	23.0	5.28 x 10^{-8}	
	2800	18.5	5.17 x 10^{-7}	
3c	1600	17.2	8.06 x 10^{-8}	10.3

If the DC field is increased to 2000 Oe (Figure 5) the high-frequency tails are suppressed and the Cole-Cole plot can be fit with a single relaxation process using CC-FIT (Figure S23 and Table S12) to give U_{eff}/k_b = 23.0 K and τ_o = 5.28 x 10^{-8} s. The alpha values are now less than 0.22 over the temperature range investigated, slightly higher than the alpha values observed in a 400 Oe DC field; the higher alpha values are likely due to the presence of a minor second relaxation process as can be seen in the very slight tails in the Cole-Cole plot. Attempts to fit the 2000 Oe data with two relaxation processes were unsuccessful. As with the measurements performed in a 400 Oe DC field the observed barrier is consistent with the U_{eff} predicted by $(S^2 - {}^1/_4)|D|$ and the energy gap between M_S states. If the applied DC field is further increased to 2800 Oe the AC data become slightly noisy and begin to broaden out at higher temperatures but a good fit can still be obtained (Figures S24, S25, S28 and Table S13), yielding U_{eff}/k_b = 18.5 K with τ_o = 5.17 x 10^{-7} s and alpha values of less than 0.36, with the highest temperature having the largest alpha value.

The observed energy barriers are consistent with those expected for an Orbach process (Table 2). However, for further verification of the Orbach pathway as the predominant one a fit including tunneling, direct, and Raman processes in addition to an Orbach process has been performed (Equation S2, Figures S30-S32 and Table S15) in the same manner as compound **1**. For all the fields the Orbach process is the predominant one, although at 400 Oe there is a small contribution from tunneling at low temperature and at 2800 Oe there is a noticeable contribution from the direct process at low temperature. Including these contributions result in slightly different energy barriers, U_{eff}/k_b = 20.5 K at 400 Oe, U_{eff}/k_b = 25.5 K at 2000 Oe and U_{eff}/k_b = 26.6 K at 2800 Oe. These energy barriers are consistent with the expected value of 24.4 K and the small increase in the energy barrier with the applied field can be due to the change in the energy of the states due to Zeeman splitting.

Compound **3c** was only investigated in an applied field of 1600 Oe, Figure 5. There are slight tails in the Cole-Cole plot but fitting the data with two relaxation processes was unsuccessful. Using a single relaxation process (Figure S26 and Table S14), an Arrhenius plot was constructed that gives U_{eff}/k_b = 17.2 K with τ_o = 8.06 x 10^{-8} s. The alpha values are less than 0.30 and the larger values are likely due to the presence of a second relaxation process, although the magnitude of the observed barrier is consistent with an Orbach relaxation mechanism. The fit including tunneling, direct, and Raman processes (Equation S2, Figure S33 and Table S15) shows a contribution from tunneling at lower temperatures and a predominance of an Orbach process at higher temperatures with an energy barrier of U_{eff}/k_b = 27.9 K, still consistent with thermal relaxation although slightly larger than the expected value of 20.6 K. One possible explanation for the different values obtained can be an overestimation of the tunneling contribution in the fit of the dependence of the relaxation time with field.

In addition, attempts to fit the dependence of τ^{-1} with temperature using only Raman and tunneling have been performed for all the compounds, however, the fits give unrealistic values for the Raman process with exponents larger than 9 and pre-exponential factors between 0.2 and 2, discarding the Raman process as a major contributor to the relaxation in this family of compounds.

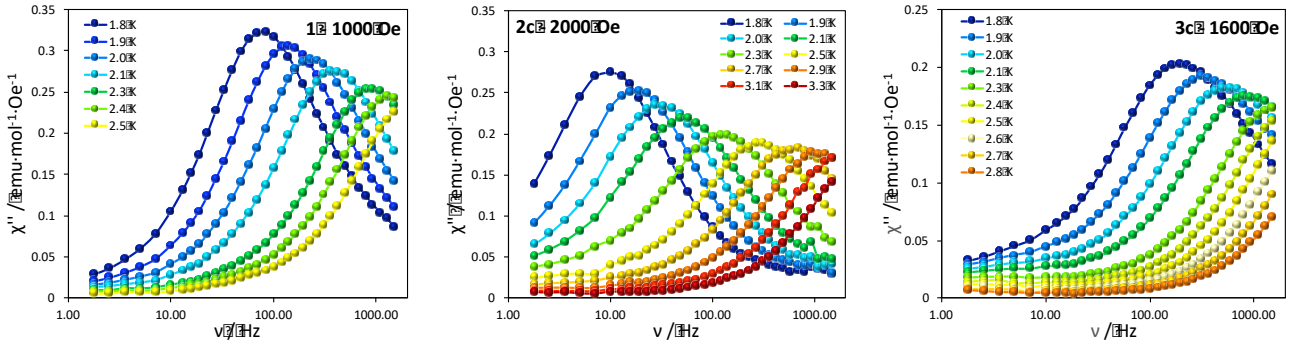

Figure 5. AC magnetic measurements for **1**, **2c** and **3c** at different temperatures and applied dc magnetic fields.

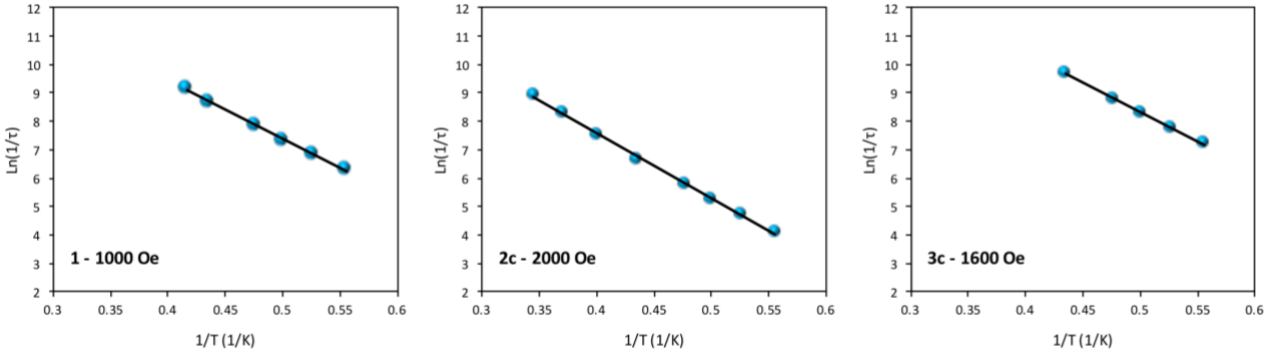

Figure 6. Arrhenius plot for **1**, **2c** and **3c** at different applied dc magnetic fields. The black line is the fit to the Arrhenius equation.

Theoretical calculations

To further investigate the different behaviors in this family of trigonal bipyramidal Co^{II} compounds theoretical calculations using the experimental geometries have been performed with Orca 3.0.3 (see SI for details). ZFS parameters at the CASSCF level are shown in Table 1 together with the experimental values obtained from the fit of the reduced magnetization. For compounds **2t**, **3t** and **4** more than one molecule is present in the asymmetric unit, so for comparison purposes the average value has been included in Table 1. The values for the different molecules and the obtained values at NEVPT2 level can be found on Table S16. It can be shown that the calculations correctly reproduce the sign of the D value, being positive only for compound **1**. For the cubic phases the E value is zero, as expected, due the symmetry of the molecule. When comparing the cubic phases with their analogous triclinic phases it can be seen that the D value is slightly smaller for the three different molecules in the triclinic phase and the E value is not zero, due to the loss of symmetry and the non-perfect C_3 axis trough the molecule (Table S16).

For a mononuclear Co^{II} compound in trigonal bipyramidal geometry the expected splitting of the d orbitals is shown in Figure 7. The sign and value of D is rationalized using the spin-orbit operator, which couples the ground and excited states.

$$\hat{H}_{SO} = \sum_i \xi_i (\hat{l}_{Zi} \cdot \hat{s}_{Zi} + \frac{1}{2}(\hat{l}_{+i} \cdot \hat{s}_{-i} + \hat{l}_{-i} \cdot \hat{s}_{+i}))$$

When the excited state results from the excitation between orbitals with the same $|m_l|$ values, the $\sum_i \hat{l}_{Zi} \cdot \hat{s}_{Zi}$ operator would couple the two orbitals, stabilizing the $M_S = \pm 3/2$ components and giving a negative contribution to the D value. When the excited state results from the excitation between orbitals with $|\Delta m_l| = 1$, the $\frac{1}{2}\sum_i \hat{l}_{+i} \cdot \hat{s}_{-i} + \hat{l}_{-i} \cdot \hat{s}_{+i}$ operator would couple the two orbitals, stabilizing the $M_S = \pm 1/2$ components and giving a positive contribution to the D value.

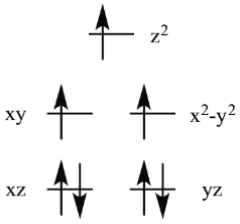

Figure 7. Schematic splitting of the d orbitals for a mononuclear Co^{II} compound in trigonal bipyramidal geometry.

For the configuration showed in Figure 7 the first excitation should involve orbitals with different m_l giving rise to a positive D value, however, as previously demonstrated by Ruamps et al. for the $[Co(Me_6tren)X]^+$ compounds their ground and excited states have a very multiconfigurational character.[4] Due to the different determinants that compose the ground and excited states, the $M_S = \pm 3/2$ level is stabilized when the ground and first excited states couple; the $M_S = \pm 1/2$

component is stabilized when ground and third or fourth excited states couple. This gives rise to an overall negative D value for the $[Co(Me_6tren)X]^+$ compounds.

Table 3. Calculated energy (cm^{-1}) and contribution to D and E values from the first 4 excited states.

Compound	State	Energy	Contrib. D	Contrib. E
1	1st ES	3635	-16.5	0.58
	2nd ES	4730	0.70	-0.58
	3rd ES	5383	11.0	11.7
	4th ES	5660	10.8	-10.8
2c	1st ES	3348	-31.9	0
	2nd ES	5040	11.0	-10.5
	3rd ES	5040	11.0	10.5
	4th ES	5516	0	0
2t	1st ES	3345	-30.9	-0.00
	2nd ES	5034	9.60	-8.24
	3rd ES	5235	9.28	6.04
	4th ES	5575	2.69	1.63

To study the difference in the sign of D between the acetonitrile compound and its halide congeners the contribution to the D value from the different excited states has been analyzed. Table 3 shows the values for compounds **1**, **2c** and the value for one of the 3 different molecules found in **2t**. The corresponding values for the other molecules in **2t**, **3c** (similar to **2c**), **3t** and **4** (similar to **2t**) can be found on Table S17. The energy difference between states is very similar for all the compounds. The energy difference between the ground and first excited state is in the range of 3300 to 3700 cm^{-1}, and the next three excited states have an energy in the range of 4700 to 5700 cm^{-1}. For the compounds in the cubic phases the second and third excited states are degenerate. For the triclinic phases, however, the second and third excited states are no longer degenerate. In the case of **1**, it seems that the order of the excited states has been flipped as the third and fourth are closer in energy and are the ones that have the largest positive contribution to the D value. Although the global D value in **1** is positive, the contribution from the first excited state is still negative as observed for the halides congeners. However, this negative contribution is smaller than in the halides congeners while the positive contributions from the other excited states are of similar magnitude for all the complexes. This leads to a global positive D value for **1** and negative D values for the halide series of compounds. The energies of the different excited states are very similar in all the compounds, which doesn't explain the smaller negative contribution to the D value in **1**. That smaller contribution may be due to the multiconfigurational character of the wavefunction and the different weight of the determinants that compose the ground state in **1** in comparison with the other compounds (Figure S34 and Table S18).

Magneto-structural correlations

If one considers only the halide series of compounds, it is reasonable to ascribe the SMM behavior of the cubic phases to the presence of strict 3-fold symmetry and the lack thereof in the triclinic phases. This symmetry argument, however, does not explain the SMM behavior of the acetonitrile complex. The bonding metrics support a similar electronic structure for all members of the family. The bond distances between the Co^{II} ion and the atom coordinated to the open site left by TPMA follow a reasonable trend, *vis*., lengthening from CH_3CN to iodide. The projection of the Co^{II} ion out of the equatorial N3 plane is similar for all of the members of the family, as are the distances and angles between the Co^{II} ion and the TPMA ligand. What is different, however, is the nearest-neighbor distance between cobalt ions. For **2t**, **3t**, and **4**, in which SMM behavior is not observed, the shortest Co···Co distance is in the range of 6.119 to 6.601 Å. For **1**, **2c**, and **3c** the shortest Co···Co intermolecular distance is in the range of 7.863 to 8.079 Å, much longer than in the triclinic halide phases. These increased cobalt distances, taken together with the narrow distribution of distances for the analogs that display similar SMM behavior, strongly suggest that dipolar interactions are the source of fast relaxation in the members of the family that do not display SMM behavior. In the $[Co(Me_6tren)Cl]ClO_4$ and $[Co(Me_6tren)Br]Br$ complexes[4] the closest Co···Co contact is 7.95 Å for the chloride complex and 8.155 Å for the bromide complex, similar to the Co···Co distances in this study. No AC susceptibility experiments were performed in this report, making a direct comparison of the SMM properties to the ones in this study impossible, but micro-SQUID measurements displayed open hysteresis loops below 1 K, thus confirming the SMM behavior of the Me_6tren complexes. A dilution study with Co:Zn ratios of 0.1:0.9 and 0.05:0.95 demonstrated that dipolar interactions were not involved in the relaxation pathway, lending support to the hypothesis that Co···Co contacts of ~8 Å are sufficient to suppress dipolar relaxation. Recently the AC magnetic behavior of $[Co(Me_6tren)Cl](ClO_4)$ was reported.[39] The complex displayed weak out-of-phase signals in a zero applied DC field and a spin reversal barrier of ~20 K across a range of applied DC fields from 2000 to 8000 Oe. This behavior is remarkable similar to that observed in the cubic phase of [Co(TPMA)Cl]Cl. In $[Co(Me_6tren)H_2O](NO_3)_2$ the closest Co···Co contact is 7.791 Å[5] but no maximum in χ'' is observable at 1.9 K, even at DC fields as high as 7000 Oe, consistent with a very fast relaxation mechanism. No investigation of the mechanism of the fast relaxation was reported. This Co···Co distance is only 0.072 Å shorter than in **1**, the SMM with the shortest Co···Co distance in this study. Since the magnitude of the dipole interaction scales as r^{-3} it is possible that this small difference in intermolecular distance is responsible for the different magnetic behavior but this seems unlikely. It has recently been shown that the interaction between the electron spin and the nuclear spin of cobalt can also have a significant impact on the relaxation properties in these types of systems,[37] as can vibronic coupling.[40] In the absence of further experimental and theoretical studies the presence of the water protons in $[Co(Me_6tren)H_2O](NO_3)_2$ leading to an increase in vibronic coupling is a much more viable explanation for the much faster relaxation observed

in $[Co(Me_6tren)H_2O](NO_3)_2$ as compared to $[Co(Me_6tren)Cl](ClO_4)$, $[Co(Me_6tren)Br]Br$, and the $[Co(TPMA)X]_+$ complexes described in this work. Also, the coordinated water molecule forms hydrogen bonds to the nitrate counteranions in that molecule. However, there are no classic hydrogen bonds between the coordinated CH_3CN molecule and the tetrafluoroborate counteranions in $[Co(TPMA)CH_3CN](BF_4)_2$.

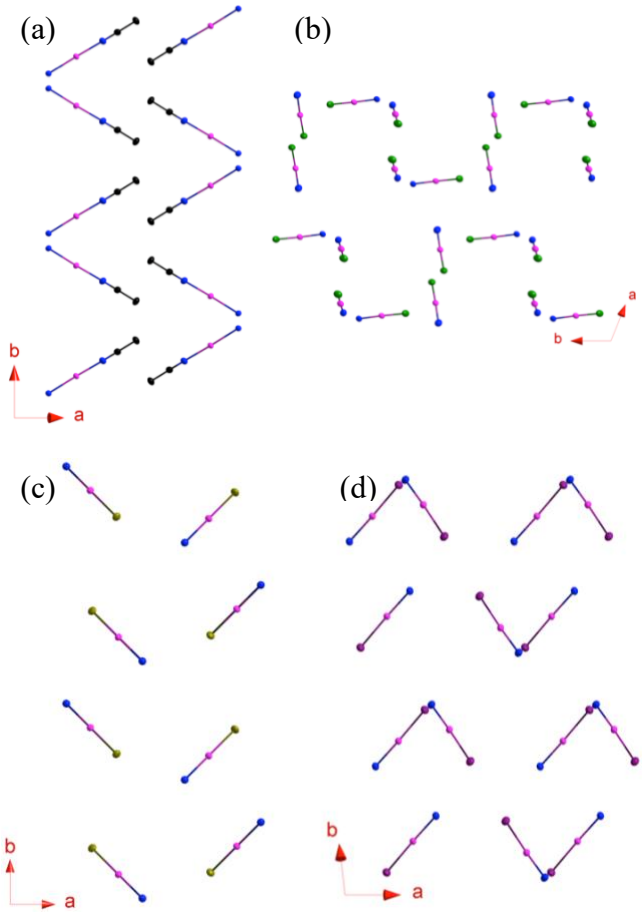

Figure 8. Packing arrangement of members of the $[Co(TPMA)X]_{n+}$ family. Only the atoms defining the C_3 axes are shown for clarity. (a) **1**. (b) **2t**. The triclinic phase of **3t** is identical. (c) **3c**. The cubic phase of **2c** is identical. (d) **4**. Color code: C, black; N, blue; Co, pink; Cl, green; Br, yellow; I, purple.

Toda esta explicación de los empaquetamientos ayuda mucho a que los referees pidan dilución o medidas en solución.

The greater flexibility of the Me_6tren ligand as compared to TPMA may also be responsible for the differences in magnetic behavior but is not thought to be a major influence given the similarity in the AC magnetic behavior of $[Co(Me_6tren)Cl](ClO_4)$ and **2c**. Transverse magnetic fields caused by the internal field of neighboring molecules has been shown to increase the tunneling probability in SMMs.[41] All of the members of this series display less than ideal packing arrangements in this respect. As can be seen in Figure 8, the C_3 axes of neighboring molecules are not co-linear in any of these molecules. Figure 8 displays schematic packing diagrams of the different members of the series as viewed down the crystallographic *c* axis. The transverse dipolar fields generated by these packing arrangements will promote quantum tunneling, explaining why a DC field is needed to observe SMM behavior even in the cubic analogs **2c** and **3c**, in which E is vanishingly small.

CONCLUSIONS

This manuscript reports the experimental a computational study of a new family of mononuclear Co^{II} compounds using the TPMA ligand, which force trigonal bipyramidal geometry, and changing the axial ligand. The CH_3CN derivate (**1**) shows a positive D value, while the halide congeners show negative D value. All the compounds have a very strong multiconfigurational character of the wavefunction and the positive D value observed in **1** arise from the smaller negative contribution of the first excited state to the D value. Only compounds **1**, **2c** and **3c** shows SMM behavior with a dependence of the relaxation time with temperature that follows Arrhenius and gives an energy barrier similar to the expected for an Orbach relaxation process, showing that no other relaxation processes are predominant for these complexes. The absence of SMM behavior for **2t**, **3t** and **4** can be attributed to the shorter Co···Co distance which produce stronger dipolar interactions allowing faster spin relaxation.

ASSOCIATED CONTENT

Supporting Information

(Word Style "TE_Supporting_Informati**on").** (Word Style "TE_Supporting_Informati**on").** A listing of the contents of each file supplied as Supporting Information should be included. For instructions on what should be included in the Supporting Information as well as how to prepare this material for publication, refer to the journal's Instructions for Authors.

The Supporting Information is available free of charge on the ACS Publications website.

brief description (file type, i.e., PDF)

brief description (file type, i.e., PDF)

AUTHOR INFORMATION

Corresponding Author

* (Word Style "FA_Corresponding_Author_Footnote"). Give contact information for the author(s) to whom correspondence should be addressed.

Present Addresses

†If an author's address is different than the one given in the affiliation line, this information may be included here.

Author Contributions

The manuscript was written through contributions of all authors. / All authors have given approval to the final version of the manuscript. / ‡These authors contributed equally. (match statement to author names with a symbol)

Funding Sources

The work performed at TAMU was supported by the National Science Foundation under Grant No. CHE-1310574. TJW thanks the Department of Energy Office of Science Graduate Fellowship Program (DOE SCGF), made possible in part by the American Recovery and Reinvestment Act of 2009, administered by ORISE-ORAU under contract No. DE-AC05-06OR23100, for fellowship support. MFBR thanks the Instituto de Ciencia y Tecnología del Distrito Federal (ICyTDF) for fellowship support. ER thanks the Spanish *Ministerio de Economía y Competitividad* (MINECO) (grant CTQ2015-64579-C3-1-P, FEDER/EU) and Generalitat de Catalunya for an ICREA Academia award. .

Notes

Any additional relevant notes should be placed here.

ACKNOWLEDGMENT

(Word Style "TD_Acknowledgments"). Generally the last paragraph of the paper is the place to acknowledge people (dedications), places, and financing (you may state grant numbers and sponsors here). Follow the journal's guidelines on what to include in the Acknowledgement section.

ABBREVIATIONS

CCR2, CC chemokine receptor 2; CCL2, CC chemokine ligand 2; CCR5, CC chemokine receptor 5; TLC, thin layer chromatography.

REFERENCES

(1) Aravena, D.; Ruiz, E. *Inorg. Chem.* **2013**, *52*, 13770.

(2) Sorace, L.; Benelli, C.; Gatteschi, D. *Chem. Soc. Rev.* **2011**, *40*, 3092.

(3) Woodruff, D. N.; Winpenny, R. E. P.; Layfield, R. A. *Chem. Rev.* **2013**, *113*, 5110.

(4) Ruamps, R.; Batchelor, L. J.; Guillot, R.; Zakhia, G.; Barra, A.-L.; Wernsdorfer, W.; Guihery, N.; Mallah, T. *Chem. Sci.* **2014**, *5*, 3418.

(5) Pinero Cruz, D. M.; Woodruff, D. N.; Jeon, I.-R.; Bhowmick, I.; Secu, M.; Hillard, E. A.; Dechambenoit, P.; Clerac, R. *New J. Chem.* **2014**, *38*, 3443.

(6) Karasawa, S.; Nakano, K.; Yoshihara, D.; Yamamoto, N.; Tanokashira, J.-i.; Yoshizaki, T.; Inagaki, Y.; Koga, N. *Inorg. Chem.* **2014**, *53*, 5447.

(7) Herchel, R.; Váhovská, L.; Potočňák, I.; Trávníček, Z. *Inorg. Chem.* **2014**, *53*, 5896.

(8) Eichhöfer, A.; Lan, Y.; Mereacre, V.; Bodenstein, T.; Weigend, F. *Inorg. Chem.* **2014**, *53*, 1962.

(9) Boča, R.; Miklovič, J.; Titiš, J. *Inorg. Chem.* **2014**, *53*, 2367.

(10) Bar, A. K.; Pichon, C.; Sutter, J.-P. *Coord. Chem. Rev.* **2016**, *308*, 346.

(11) Gómez-Coca, S.; Aravena, D.; Morales, R.; Ruiz, E. *Coord. Chem. Rev.* **2015**, *289-290*, 379.

(12) Huang, X.-C.; Zhou, C.; Shao, D.; Wang, X.-Y. *Inorg. Chem.* **2014**, *53*, 12671.

(13) Chen, L.; Wang, J.; Wei, J.-M.; Wernsdorfer, W.; Chen, X.-T.; Zhang, Y.-Q.; Song, Y.; Xue, Z.-L. *J. Am. Chem. Soc.* **2014**, *136*, 12213.

(14) Rechkemmer, Y.; Breitgoff, F. D.; van der Meer, M.; Atanasov, M.; Hakl, M.; Orlita, M.; Neugebauer, P.; Neese, F.; Sarkar, B.; van Slageren, J. *Nat. Commun.* **2016**, *7*.

(15) Zadrozny, J. M.; Xiao, D. J.; Atanasov, M.; Long, G. J.; Grandjean, F.; Neese, F.; Long, J. R. *Nat. Chem.* **2013**, *5*, 577.

(16) Zadrozny, J. M.; Atanasov, M.; Bryan, A. M.; Lin, C.-Y.; Rekken, B. D.; Power, P. P.; Neese, F.; Long, J. R. *Chem. Sci.* **2013**, *4*, 125.

(17) Mossin, S.; Tran, B. L.; Adhikari, D.; Pink, M.; Heinemann, F. W.; Sutter, J.; Szilagyi, R. K.; Meyer, K.; Mindiola, D. J. *J. Am. Chem. Soc.* **2012**, *134*, 13651.

(18) Poulten, R. C.; Page, M. J.; Algarra, A. G.; Le Roy, J. J.; López, I.; Carter, E.; Llobet, A.; Macgregor, S. A.; Mahon, M. F.; Murphy, D. M.; Murugesu, M.; Whittlesey, M. K. *J. Am. Chem. Soc.* **2013**, *135*, 13640.

(19) Lin, W.; Bodenstein, T.; Mereacre, V.; Fink, K.; Eichhöfer, A. *Inorg. Chem.* **2016**, *55*, 2091.

(20) Miklovič, J.; Valigura, D.; Boča, R.; Titiš, J. *Dalton Trans.* **2015**, *44*, 12484.

(21) Chilton, N. F.; Anderson, R. P.; Turner, L. D.; Soncini, A.; Murray, K. S. *J. Comput. Chem.* **2013**, *34*, 1164.

(22) Cole, K. S.; Cole, R. H. *J. Chem. Phys.* **1941**, *9*, 341.

(23) Aubin, S. M. J.; Sun, Z.; Pardi, L.; Krzystek, J.; Folting, K.; Brunel, L.-C.; Rheingold, A. L.; Christou, G.; Hendrickson, D. N. *Inorg. Chem.* **1999**, *38*, 5329.

(24) Zhu, Y.-Y.; Cui, C.; Zhang, Y.-Q.; Jia, J.-H.; Guo, X.; Gao, C.; Qian, K.; Jiang, S.-D.; Wang, B.-W.; Wang, Z.-M.; Gao, S. *Chem. Sci.* **2013**, *4*, 1802.

(25) Zadrozny, J. M.; Telser, J.; Long, J. R. *Polyhedron* **2013**, *64*, 209.

(26) Huang, W.; Liu, T.; Wu, D.; Cheng, J.; Ouyang, Z. W.; Duan, C. *Dalton Trans.* **2013**, *42*, 15326.

(27) Habib, F.; Luca, O. R.; Vieru, V.; Shiddiq, M.; Korobkov, I.; Gorelsky, S. I.; Takase, M. K.; Chibotaru, L. F.; Hill, S.; Crabtree, R. H.; Murugesu, M. *Angew. Chem. Int. Ed.* **2013**, *52*, 11290.

(28) Zadrozny, J. M.; Liu, J.; Piro, N. A.; Chang, C. J.; Hill, S.; Long, J. R. *Chem. Commun.* **2012**, *48*, 3927.

(29) Karasawa, S.; Nakano, K.; Tanokashira, J.-i.; Yamamoto, N.; Yoshizaki, T.; Koga, N. *Dalton Trans.* **2012**, *41*, 13656.

(30) Buchholz, A.; Eseola, A. O.; Plass, W. *Comptes Rendus Chimie* **2012**, *15*, 929.

(31) Zadrozny, J. M.; Long, J. R. *J. Am. Chem. Soc.* **2011**, *133*, 20732.

(32) Yoshihara, D.; Karasawa, S.; Koga, N. *Polyhedron* **2011**, *30*, 3211.

(33) Karasawa, S.; Koga, N. *Inorg. Chem.* **2011**, *50*, 5186.

(34) Jurca, T.; Farghal, A.; Lin, P.-H.; Korobkov, I.; Murugesu, M.; Richeson, D. S. *J. Am. Chem. Soc.* **2011**, *133*, 15814.

(35) Vallejo, J.; Castro, I.; Ruiz-García, R.; Cano, J.; Julve, M.; Lloret, F.; De Munno, G.; Wernsdorfer, W.; Pardo, E. *J. Am. Chem. Soc.* **2012**, *134*, 15704.

(36) Wu, D.; Zhang, X.; Huang, P.; Huang, W.; Ruan, M.; Ouyang, Z. W. *Inorg. Chem.* **2013**, *52*, 10976.

(37) Gómez-Coca, S.; Urtizberea, A.; Cremades, E.; Alonso, P. J.; Camón, A.; Ruiz, E.; Luis, F. *Nat. Commun.* **2014**, *5*.

(38) Chilton, N. F.; Nicholas F. Chilton: 2014.

(39) Packová, A.; Miklovič, J.; Boča, R. *Polyhedron* **2015**, *102*, 88.

(40) Atanasov, M.; Zadrozny, J. M.; Long, J. R.; Neese, F. *Chem. Sci.* **2013**, *4*, 139.

(41) Glaser, T.; Hoeke, V.; Gieb, K.; Schnack, J.; Schröder, C.; Müller, P. *Coord. Chem. Rev.* **2015**, *289–290*, 261.